HAL
open science

Carbon nanotubes, but not spherical nanoparticles, block autophagy by a shape-related targeting of lysosomes in murine macrophages

Vanessa Cohignac, Marion Julie Landry, Audrey Ridoux, Mathieu Pinault, Balasubramanyam Annangi, Adèle Gerdil, Nathalie Herlin-Boime, Martine Mayne, Masatake Haruta, Patrice Codogno, et al.

To cite this version:

Vanessa Cohignac, Marion Julie Landry, Audrey Ridoux, Mathieu Pinault, Balasubramanyam Annangi, et al.. Carbon nanotubes, but not spherical nanoparticles, block autophagy by a shape-related targeting of lysosomes in murine macrophages. Autophagy, 2018, 14, pp.1474993. 10.1080/15548627.2018.1474993 . cea-01823746

HAL Id: cea-01823746

https://cea.hal.science/cea-01823746v1

Submitted on 6 Jul 2018

HAL is a multi-disciplinary open access archive for the deposit and dissemination of scientific research documents, whether they are published or not. The documents may come from teaching and research institutions in France or abroad, or from public or private research centers.

L'archive ouverte pluridisciplinaire **HAL**, est destinée au dépôt et à la diffusion de documents scientifiques de niveau recherche, publiés ou non, émanant des établissements d'enseignement et de recherche français ou étrangers, des laboratoires publics ou privés.

Carbon nanotubes, but not spherical nanoparticles, block autophagy by a shape-related targeting of lysosomes in murine macrophages

Vanessa Cohignac[1,2*], Marion Julie Landry[1,2*], Audrey Ridoux[1], Mathieu Pinault[3], Balasubramanyam Annangi[1,2], Adèle Gerdil[3], Nathalie Herlin-Boime[3], Martine Mayne[3], Masatake Haruta[4], Patrice Codogno[5,6], Jorge Boczkowski[1,2,7], Jean-Claude Pairon[1,2,8] and Sophie Lanone[1,2#]

[1]Inserm U955, Institut Mondor de Recherche Biomédicale (IMRB) Equipe 04, Créteil, France

[2]Université Paris Est-Créteil, Faculté de Médecine, Créteil, France

[3]NIMBE, CEA, CNRS, Université Paris-Saclay, CEA Saclay 91191 Gif sur Yvette Cedex, France

[4]Research Center for Gold 1-1 Minami Osawa Hachioji, Tokyo 192-0397, Tokyo Metropolitan University, Japan

[5]Inserm U1151 CNRS UMR 8253, Institut Necker-Enfants Malades, Paris (INEM), France

[6]Université Paris Descartes-Sorbonne Paris Cité, Paris, France

[7]DHU A-TVB, Antenne de Pneumologie, Service de Réanimation Médicale Assistance Publique-Hôpitaux de Paris, Hôpitaux Universitaires Henri Mondor, 51 Avenue du Maréchal de Lattre de Tassigny, 94010 Créteil CEDEX, France

[8]Centre Hospitalier Intercommunal, Service de pneumologie et pathologie professionnelle, Créteil, France

* Equal contribution

Corresponding author:

Sophie Lanone

Inserm U955, Institut Mondor de Recherche Biomédicale (IMRB), Equipe 04

Faculté de Médecine de Créteil

8 rue du Général Sarrail

Keywords: autophagy, carbon nanotubes, lysosomes, physico-chemical characteristics, titanium dioxide.

Abbreviations: Au, gold; Baf-A1, bafilomycin A_1; CNT, carbon nanotube; Fe_xO_y, iron oxide; GFP, green fluorescent protein; LAMP, lysosomal-associated membrane protein; LC3, microtubule-associated protein 1 light chain 3; L-CNT, long carbon nanotube; LF-CNT, long functionalized carbon nanotube; MWCNT, multi-walled carbon nanotube; Noco, nocodazole; NP, nanoparticle; Rapa, rapamycin; RFP, red fluorescent protein; ROS, reactive oxygen species; S-CNT, short carbon nanotube; SF-CNT, short functionalized carbon nanotube; Stx17, syntaxin 17; SNAP29, synaptosomal-associated protein 29; SWCNT, single-walled carbon nanotube; TEM, transmission electron microscopy; TiO_2, titanium dioxide; VAMP8, vesicle-associated membrane protein 8; XRD, X-ray diffractometer

Abstract

Nanoparticles (NPs) can be toxic, depending on their physico-chemical characteristics. Macroautophagy/autophagy could represent a potential underlying mechanism of this toxicity. We therefore set up a study aimed to characterize in depth the effects, on autophagy, of macrophage exposure to NPs, with a particular attention paid to the role of NP physico-chemical characteristics (specifically chemical composition, shape, size, length, crystal phase, and/or surface properties). We demonstrate that exposure to carbon nanotubes (CNT) but not to spherical NPs leads to the blockage of the autophagic flux. We further identified lysosomal dysfunction, in association with the downregulation of SNAPIN expression, as the underlying mechanism responsible for the CNT-induced autophagy blockade. These results identify for the first time the shape as a major determinant of the interaction of NPs with the autophagy pathway. Moreover, identifying the lysosomes and SNAPIN as primary targets of MWCNT toxicity opens new directions in the interpretation and understanding of nanomaterial toxicity.

Introduction

Engineered nanomaterials, including carbon nanotubes (CNT) and metal nanoparticles (NPs), have already widespread applications in various industrial fields; they are utilized in electronics, optics, cosmetics, food products, drug delivery etc. Because engineered nanomaterials became part of our everyday life, there has been an increasing concern regarding the health consequences that could result from human exposure to these nanomaterials. A large body of studies, performed *in vitro* in cells or *in* vivo in laboratory animals has now been published showing evidence that engineered nanomaterials can exert harmful effects [1, 2], with the generation of oxidative stress and the development of an inflammatory response as the most commonly accepted underlying mechanisms. For example at the respiratory level, which is considered as a major exposure route, CNT or titanium dioxide (TiO_2) NPs are able to induce lung remodeling, consistent with fibrosis and/or the development of granulomas [3, 4]. However, these effects are not always described, and, if the physico-chemical characteristics of the nanomaterials are often proposed as important determinants of their toxic effects, the exact ins and outs of nanomaterial toxicity are not yet completely understood [5, 6].

Autophagy is a physiological process aimed to maintain cellular homeostasis, in which cytoplasmic components are digested via a lysosomal pathway. During this process, a portion of cytoplasm is engulfed by a double-membrane structure called the phagophore, which matures into an autophagosome that subsequently fuses with a lysosome, leading to the formation of an autolysosome, where the degradation of the enclosed materials by lysosomal enzymes can occur [7]. Autophagy plays a key role in various pathological processes, such as cancer, or cardiovascular and pulmonary diseases [8]. The involvement of autophagy in these diseases could be linked to its role in the downregulation of oxidative stress and inflammatory responses [9]. Because NPs could end up in lysosomes, the terminal organelle of autophagy,

and given that oxidative stress and inflammatory responses are 2 major mechanisms underlying NP toxicity, a dysfunction of the autophagy process could represent a new mechanism explaining, at least in part, NP toxicity [10].

A few studies have been published so far regarding the effects of cellular exposure to NPs on the autophagy process [11]. From these studies, it is currently not clear whether these nanomaterials (metal oxide NPs such as TiO_2, and Fe_xO_y, or carbonaceous ones such as carbon black, graphene or CNT) induce or block autophagy [11-15]. Surprisingly, almost none of these studies have been performed in macrophages, although this cell type is particularly relevant to the interaction with NPs and their processing [16]. Moreover, although the physico-chemical characteristics of nanomaterials are known to be important determinants of their toxicity, only a few studies addressed this issue with regard to the autophagy process. For example, Yu *et al* have shown that pristine multi-walled CNT (MWCNT), but not acid-functionalized ones, induce an abnormal accumulation of autophagosomes, probably because of an autophagy blockade [12]. Moreover, TiO_2 NP can induce an increase of the autophagic flux, not observed with iron or zinc oxide NP of similar size, suggesting that the chemical nature of NP could differentially impact the autophagy process [17]. However, the specific relevance of each of the physico-chemical characteristics of NPs on their effect on autophagy is currently far from understood and certainly deserves more systematic investigations.

Therefore, the global aim of the present study was to evaluate the effects of macrophage exposure to NPs on autophagy, with a particular attention paid to the role of NP physico-chemical characteristics in this process. We specifically focused on carbon- and titanium-based nanomaterials, because of their already wide production and use. Therefore, RAW 264.7 murine macrophages were exposed to carbonaceous (MWCNT or carbon black) or metal oxide (TiO_2) NP, varying in shape (tubular or spherical), length (short or long CNT), size (nano or micro TiO_2), crystal phase (anatase and/or rutile TiO_2), or surface properties

(pristine or acid-functionalized CNT, and Au grafting on TiO_2 NP). Overall, the effects of 12 nanomaterials were investigated: 4 MWCNT (short, short functionalized, long and long functionalized; S-, SF-, L-, and LF-CNT respectively), 1 carbon black NP (FW2), 1 micrometric TiO_2 (Micro) and 6 TiO_2 NP (A10, A/R, Rut, P25, P25-Au3, P25-Au8). Our data overall show that macrophage exposure to CNT, but not to spherical NP (C- or Ti-based) blocks the autophagy flux, via the alteration of lysosomal function, possibly through the downregulation of SNAPIN expression, leading to the absence of autophagosome fusion with lysosomes.

Results

Characterization of particles

A full physico-chemical characterization of the 4 different CNT used in this study has been provided elsewhere [18]. Briefly, typical transmission electron microscopy (TEM) images of the different nanomaterials are presented in Figure 1A. The 4 MWCNT present the typical tubular morphology of nanotubes, and all TiO_2 particles were spherical except the rutile one (Rut), which was needle-like (Figure 1A). As expected, the 4 MWCNT presented a similar diameter and a shorter length for S- and SF-CNT as compared to L- and LF-CNT (Table 1). The physico-chemical characteristics of the different particles are summarized in Table 1. The crystal phase of TiO_2 particles was assessed by X-ray diffraction analysis: in accordance with the manufacturers' data, A10 and Micro were 100% anatase, Rut was 100 % rutile and A/R and P25-based NP were a mix of anatase and rutile (with an anatase:rutile ratio of 13:7 and 4:1, respectively). Particle morphology and chemical composition were confirmed using scanning electron microscopy coupled to an energy dispersive X-ray (analysis (data not shown). Thermogravimetric analysis showed that the average iron content was roughly similar for non-functionalized CNT (4.4 and 4.5 wt% for S- and L-CNT, respectively), and for the functionalized ones (1.3 and 1.0 wt% for SF- and LF-CNT, respectively). No other trace element could be detected [18]. All particles, except micrometric TiO_2 (Micro), present a surface area over 20 m^2/g. For all particle suspensions, except for the rutile one, the zeta potential was lower than |25| mV, a commonly admitted limit above which the suspension is stable, indicating that the suspensions could be agglomerated. This was confirmed by the measurement of hydrodynamic diameter, with values between 54 and 1033 nm. Endotoxin levels were below the detection limit for all particles. Finally, S-, L- and LF-CNT were the most potent particles to generate ROS in acellular conditions, whereas SF-CNT, FW2 and Rut did not produce any detectable ROS.

All particles are internalized by macrophages in vitro

Figure 1B shows representative TEM images of macrophages exposed for 6 h to the different particles. All particles could be internalized by macrophages, which was also confirmed by the absence of an inhibitory effect on the phagocytic capacity of the macrophages, whatever the particle tested (Figure S1). Internalized particles were present mainly inside vacuoles. No particle was found in the nucleus or mitochondria of the treated cells. In addition, mitochondria, endoplasmic reticulum and Golgi apparatus did not show any obvious sign of morphological alteration, overall suggesting an absence of NP-induced toxicity. This was confirmed by the absence of modification in mitochondrial activity or DNA content, whatever the treatment of the cells up to 50 µg/ml (Figure S2A and S2B). Therefore, we chose to expose cells to 50 µg/ml of particles, taken as a non-cytotoxic dose.

Exposure to TiO_2 NP induces autophagy, whereas exposure to MWCNT inhibits autophagic flux

To elucidate the effect of MWCNT and TiO_2 NPs on the autophagic process, we first examined the accumulation of autophagosomes in macrophages exposed to the different particles for 6 h or to rapamycin, a positive control of autophagy induction, by the quantification of MAP1LC3-II/LC3-II (microtubule-associated protein 1 light chain 3) protein expression. As shown in Figure 2A and 2B, all particles induced a significant increase of LC3-II protein expression in macrophages, attesting to autophagosome accumulation. Enhanced LC3-II levels could be the result of either an increased autophagosome synthesis (induction of autophagy) or of a decreased autophagosome turnover (blockade of autophagic flux). To distinguish between these 2 opposite scenarios, we investigated the expression of LC3-II in the presence of autophagy inhibitors, such as bafilomycin A_1 (Baf-A1), a specific

vacuolar-type H^+-translocating ATPase inhibitor. We show that MWCNT-induced accumulation of LC3-II was not enhanced in presence of the inhibitor, suggesting that exposure to MWCNT blocks autophagic flux. Conversely, the accumulation of LC3-II observed in response to the other particles (FW2, Micro and TiO_2 NP) was upregulated in the presence of Baf-A1, suggesting that these particles were able to induce a functional autophagy (Figure 2C and 2D). Similar results were obtained in primary macrophages (Figure S3).

In order to definitively conclude on the effects of particle exposure on the autophagic flux, we used the GFP-mRFP-LC3 plasmid transfection in macrophages. This probe is used to identify and differentiate autophagosomes (GFP^+ and RFP^+, seen as yellow dots) from autolysosomes (GFP^- and RFP^+, seen as red dots) thanks to the quenching of GFP fluorescence in acidic compartments [19]. Confocal images of rapamycin-treated macrophages, but also of cells exposed to FW2, Micro and TiO_2 NP, showed an increase of total autophagic structures together with an increase of autolysosome number as compared to what was found in unexposed cells, consistent with the induction of a functional autophagy (Figure 3A and 3B). Conversely, exposure to MWCNT was associated with a Baf-A1-like phenotype, with an increase of the total number of autophagic structures in absence of an increase of autolysosome number, confirming the blockade of the autophagic flux in response to these particles. Overall, these results suggest that exposure to spherical particles induces autophagy, whereas exposure to MWCNT inhibits autophagic flux. The following experiments were dedicated to understand the mechanism(s) underlying CNT inhibition of autophagic flux.

Macrophage exposure to CNT impairs autophagosome fusion with lysosomes

An impairment of the fusion between autophagosomes and lysosomes could explain the perturbations in the autophagic flux observed in response to CNT [10]. Confocal images of

MWCNT-exposed macrophages showed an absence of colocalization of LC3 with LAMP1 (lysosomal-associated membrane protein 1) immunofluorescence, indicating an absence of fusion between autophagosomes and lysosomes in these experimental conditions. A correct fusion of autophagosomes with lysosomes could be observed in macrophages exposed to FW2 or P25, the 2 spherical NP taken as positive controls of autophagy induction (Figure 4A and 4B). Similarly, the level of the autophagy cargo SQSTM1/p62 (sequestosome 1) was found increased in response to all 4 CNT, whereas not in response to FW2 or P25 (Figure S4).

Because, microtubules are essential to the transport of autophagosomes to lysosomes, we next examined the cytoskeleton structure by TUBA/α-tubulin immunostaining [20]. As expected, Figure S5A showed the disruption of the microtubule network when cells were treated with nocodazole, an inhibitor of microtubule polymerization. However, no disruption of the microtubule network was observed after exposure of RAW macrophages to CNT, FW2 or P25. Moreover, we also observed no change in the actin cytoskeleton (Figure S5B). Furthermore, the overall gene expression of several SNARE proteins (STX17 [syntaxin 17), SNAP29 [synaptosomal-associated protein 29], and VAMP8 [vesicle-associated membrane protein 8]) that mediate autophagosome-lysosome fusion [21] was not modified by any exposure to particles (data not shown). These experiments strongly suggest that the impairment of fusion between autophagosomes and lysosomes induced by CNT exposure is not related to an impairment of the expression of the fusion machinery between autophagosomes and lysosomes.

Exposure to MWCNT induces lysosomal alterations

Lysosomal function is essential to ensure a correct autophagic flux [14, 22]. Therefore, we next investigated lysosomes as potential targets of MWCNT. Acridine orange staining showed a lack of acidification in response to all CNT, whereas exposure to rapamycin (used

as a positive control), FW2 or P25 did not impair the acidification of the lysosomal compartment (Figure 5A and 5B), thus indicating an alteration of lysosomal function in response to CNT. Finally, as SNAPIN (SNAP-associated protein), an adaptor protein in the SNARE/soluble NSF attachment protein alpha core complex, has been recently demonstrated to be critical for lysosomal acidification and autophagosome maturation in macrophages [23], we next investigated its expression after exposure of RAW macrophages to the different particles. As shown in Figure 6A and 6B, macrophage exposure to CNT, but not to FW2 or TiO_2 NP led to a decreased expression of SNAPIN, which could be related to the lack of lysosomal acidification in these conditions. This was also accompanied by an accumulation of LAMP-positive compartments (Figure S6), suggesting an increase in lysosome number [24].

Discussion

Overall, our results show that the effect of carbon- and titanium-based nanomaterials on the autophagy process is dependent on their physico-chemical characteristics, and mainly that of their shape (nanoparticles versus tubes). Moreover, we provide the first evidence that lysosomal dysfunction is the molecular mechanism underlying autophagy blockade by MWCNT, potentially via the modulation of SNAPIN expression.

The role of 6 different physico-chemical characteristics on autophagosome accumulation was addressed in our experimental setting: chemical composition, shape, length, size, crystal phase, and surface properties. In light of our results, the shape (tubular for CNT versus spherical for the other carbon- or titanium-based nanomaterials) seems to be the most important characteristic to overall induce or block autophagy. Indeed, tubular nanomaterials (MWCNT) induce a blockade of autophagic flux, whereas macrophage exposure to spherical particles (FW2 and TiO_2 nano or microparticles) leads to the activation of a functional autophagy. Interestingly, Rutile NP, which presents a needle-like shape, did not behave like CNT in regard to autophagy. This could be related to their different chemical composition (titanium versus carbon). However, when used as a spherical NP, carbon (FW2) and TiO_2 NP have similar effects. More probably, the specific effect of CNT as opposed to Rutile NP is the result of very different diameter:length ratio between them: 1:4 for Rutile NP, and 1:30 or up to 1:65 for S/SF- or L/LF-CNT, respectively. Indeed, this parameter can highly affect the particle-cell interactions, and could be particularly important in our experimental setting [25]. The literature reports only a few experimental studies so far regarding the effects of CNT on autophagosome accumulation. Wan and colleagues identified the accumulation of LC3-II in murine macrophages exposed to SWCNT in vitro [26]. Similarly, Yu and colleagues demonstrate that pulmonary exposure of mice to pristine but not acid-functionalized MWCNT induces the accumulation of LC3-II in the lungs of the animals [12]. Although we cannot

strictly compare the 2 studies because of the specificity of each CNT in terms of functionalization, the results obtained by Yu et al. slightly differ from ours, as we did not observe any impact of CNT surface modifications; exposure to either functionalized or pristine CNT (SF- or LF- versus S- or L-CNT) results in a similar LC3-II accumulation. A comparable lack of effect of surface modification was observed for TiO_2 NP: Au grafting on P25 NP did not modify the overall autophagy induction by pristine P25 NP. It is important to note however that the studies by Yu or Wan only evaluated LC3-II (and SQSTM1) accumulation, which is far from sufficient to draw a definitive conclusion on autophagic flux modulation [27].

In an attempt to identify the underlying mechanism that could explain the absence of autophagosome maturation in response to MWCNT exposure, we failed to detect any modification of the cytoskeleton network as well as any modulation in the expression levels of several proteins implicated in the fusion between autophagosomes and lysosomes. These results, which could be linked to the absence of phagocytosis modulation that we observed in response to MWCNT [28], are in accordance with data from the literature, which does not systematically report an impact of CNT on cellular cytoskeleton [29]. However, we identified lysosomal alteration as the mechanism linked to the absence of autophagosome maturation, characterized by a lack of lysosomal acidification in response to all CNT. More specifically, we observed for the first time that macrophage exposure to CNT leads to the downregulation of SNAPIN expression, a protein initially isolated in neurons [30]. Silencing of *SNAPIN* in primary human macrophages has been recently shown leading to an incomplete lysosomal hydrolysis as well as an impaired autophagy flux, thus identifying SNAPIN as critical for the maintenance of healthy lysosomes and autophagy [23]. In macrophages from rheumatoid arthritis (RA) patients, SNAPIN has been identified as a potential endogenous TLR2 (toll like receptor 2) ligand, possibly contributing to the pathogenesis of the disease [31]. Although the

exact interplay between CNT and TLRs is complex and currently not entirely understood [32], both CNT and TiO2 NP activate TLR2 signaling [33-35] suggesting that the effects of CNT on SNAPIN expression we observed in the present study might not be the result of the modulation of TLR2 signaling by CNT. Further studies identifying the signaling pathway leading to SNAPIN expression are needed to fully understand how CNT exert their effects.

Our study overall demonstrates that macrophage exposure to MWCNT leads to a non-functional autophagy process, secondary to the alteration of lysosomal function, via the downregulation of SNAPIN expression. Moreover, this identifies for the first time the shape of nanomaterials, and neither their surface modification, nor length, as the essential physico-chemical characteristic determining lysosomes as the primary target of MWCNT toxicity. Deciphering such interactions opens new ways in the interpretation and understanding of nanomaterial toxicity.

Materials and methods

Production of particles

The MWCNT were synthetized as previously described [18]. Briefly, the initial aligned multi-walled CNT powder (at the gram scale) was produced by aerosol-assisted catalytic chemical vapor deposition [36]. This method is based on the catalytic decomposition of liquid hydrocarbons by injecting mixed aerosols containing both the hydrocarbon and the metallic sources, which simultaneously and continuously fill the reactor. A solution composed of ferrocene dissolved in toluene (1.25 wt. %) was used to synthesize the nanotube samples at 800°C under Ar-H_2 atmosphere (70:30 vol. %). The duration of the growth was set at 45 min. The presence of dihydrogen in the vector of the aerosol made it possible to obtain a small external diameter, as previously described by Castro et al [36]. Following this procedure, the sample was formed of aligned CNT carpets covering the reactor walls. Once detached from the reactor walls by scraping, the precursor sample was treated in de-ionized water (Millipore, 18.2 MΩ.cm, 848333), with a dispersing agent (1 wt. % biliary salts [Sigma, T-110], composed of 50 wt.% sodium deoxycholate [≥ 98 wt. %; Acros Organics, 218591000], 50 wt. % sodium cholate [99 wt. %; Acros Organics, MFCD00064138]). An ultrasonic probe, Bioblock Vibracell 75043 (Bioblock) working at 20 kHz and 375 W in pulse mode (1s/1s amplitude, 50% power) was used to control the CNT shortening and reach a desired length distribution [37]. Different ultrasonic treatment durations were applied to obtain 2 distinct groups of CNT: a short group and a long group, after respectively 7 h and 5 min of ultrasound. Both CNT powders were purified at 1000°C under Ar atmosphere after filtration in order to remove/burn traces of dispersing reagent. The 2 dry samples were then separated in 2 subgroups. One subgroup of each group was treated with acidic solution (75 wt. % H_2SO_4, 25 wt. % HNO_3) at 60°C for 2 h to functionalize the nanotubes by grafting oxidized groups on their surface. Finally, the different subgroups were extensively washed with de-

ionized water, and final dry samples of CNT were obtained by evaporating water in a fume hood. Ultimately, 4 distinct groups were obtained, with controlled length and surface chemistry: short (S-CNT), short functionalized (SF-CNT), long (L-CNT) and long functionalized (LF-CNT).

The other particles were purchased from different suppliers: A10 (TiO_2) and Rut (TiO_2) were obtained from Nanostructured & Amorphous Materials (5417HT and 5484WJ respectively); A/R (TiO_2) was supplied by Sigma Aldrich (634662); P25 (TiO_2) and FW2 (CB) were supplied by Evonik Industries (Aeroxide® TiO_2, P25 and FW200, respectively); and Micro (TiO_2) was obtained from Acros organics (21358). P25 - Au3 (P25 with 1 wt. % of Au NPs of 3 nm of diameter grafted on its surface) and P25 - Au8 (P25 with 1 wt. % of Au NPs of 6 nm of diameter grafted on its surface) were kindly provided by Professor Matasake Haruta (Tokyo Metropolitan University, Japan) [38].

Physicochemical characterization of the particles

The size, size distribution and zeta potential of the particles suspended in water were measured by dynamic light scattering using a ZetaSizer HS 3000 (Malvern Instrument, Worcestershire, United Kingdom). Particle size and shape were also characterized by TEM using Philips CM12 instrument (Amsterdam, Netherlands) at an accelerating voltage of 80 kV. Particle morphology and composition were confirmed using scanning electron microscopy (Carl Zeiss Ultra 55, Oberkochen, Germany) coupled to an energy-dispersive X-ray system (EDX) (Bruker, Billerica, MA). For TiO_2 particles, crystallinity was determined using a X-ray diffractometer (XRD) (Siemens D5000, Munich, Germany). The measurement of the specific surface area of the particles was carried out by a Micromeritics Flowsorb 2300 (Norcross, GA) using the Brunauer Emmett Teller (BET) analysis. For the MWCNT, thermogravimetric analysis was performed with a TGA 92–16, 18 Setaram apparatus

(Setaram Instrumentation, France) under flowing air at a temperature up to 1000°C (10°C/min heating ramp) to determine the sample initial iron content by measuring the remaining iron oxide weight.

Particles were assessed for endotoxin contamination using the Limulus Amebocyte Lysate assay (Lonza, Bâle, Switzerland), performed as recommended by the manufacturer.

The intrinsic production of ROS by particles was measured in acellular conditions using the properties of φX174 RFI plasmid DNA (Thermo Fisher Scientific, SD0031). This DNA has the ability to decoil in the presence of ROS. Plasmid DNA (290 ng) were mixed with 100 µg/mL of particles for 8 h at 37°C [39]. The PstI endonuclease (Thermo Fisher Scientific, ER0615) was used as a positive control. The different forms of DNA in the samples (coiled, decoiled and linearized) were then separated on an agarose gel (0.8 wt. %) for 16 h at 30 mV. The intensity of the different DNA bands was quantified, and the ratio of the decoiled and linearized DNA intensity to the total DNA intensity was calculated.

Particle suspensions preparation

Stock suspensions of particles (2 mg/ml) were prepared in Dulbecco's modified Eagle medium (DMEM; Life Technologies, 11995065) and stored at -20°C until use. Stock suspensions were diluted in DMEM supplemented with 1 vol. % of antibiotics (penicillin-streptomycin; Life Technologies, 15140148) without fetal bovine serum (FBS) and sonicated for 15 min just before cell exposure.

Cell culture

A murine macrophage cell line, RAW264.7 was used in this study (ATCC, TIB-71). Cells were grown in DMEM cell culture medium supplemented with 10 vol. % of FBS and 1 vol. % of antibiotics (penicillin-streptomycin). Cells were cultured on plastic material and were

maintained at 37°C in a humidified atmosphere containing 5% vol. CO_2. Subconfluent cell cultures were exposed for 6 h to 10-100 µg/ml of particles in DMEM in the absence of FBS. For some experiments, cells were treated with Baf-A1 (100 nM; Sigma Aldrich, B1793), chloroquine (CQ; 100 µM, Sigma Aldrich, C6628) during 2 h before the end of particle exposure or with rapamycin (Rapa, 100 nM; Sigma Aldrich, R8781) during the duration of the experiment. All experiments were performed using cells between passages 4 and 15.

A subset of experiments were performed on murine primary peritoneal macrophages, that were obtained as previously described [40].

Cell viability assay

Two methods were used to evaluate changes in cell viability: the mitochondrial activity assay (WST-1 assay; Roche Diagnostics, 5015944001) and the quantification of DNA content (Hoechst assay; Sigma-Aldrich, 33342). For each method, cells were seeded on 96-well plates and left to settle during 24 h. Cells were then exposed to a scaling dose of particles (10-100 µg/ml) during 6 h. Exposure to 10 vol. % Triton X-100 (Sigma-Aldrich, X100) was used as a positive control. These tests were performed following the manufacturer's instructions. The cell viability was expressed as a percentage of the viability of the control cells.

Phagocytosis assay

RAW 264.7 cells (ATCC) were exposed to 50 µg/mL CNT for 6 h, together with Latex beads-rabbit IgG-FITC complex, as per the manufacturer's instructions (Phagocytosis assay Kit; Cayman Chemical, 500290). Fluorescence was measured at λ_{exc} = 485 nm, and λ_{emi} = 535 nm.

Ultrastructural analysis

Internalization of particles and morphology of cells were studied using TEM. After 6-h treatment with 50 µg/ml of particles, cells were fixed with 2 vol. % gluteraldehyde in 0.1 M sodium cacodylate buffer, pH 7.4, post-fixed in 1 vol. % osmium and embedded in Epon (Sigma, 45345). Ultrafine sections (90-nm thick) were collected on copper grids (Sigma, G4776), stained with uranyl acetate and lead citrate and observed using a JEOL 1400 transmission electron microscope at an accelerating voltage of 80 kV.

Real-time polymerase chain reaction (RT-PCR)

Total mRNA was isolated from exposed cells (50 µg/ml of particles during 6 h) using the RNeasy kit (Qiagen, 74104). Reverse transcription reactions were performed with Moloney murine leukemia virus reverse transcriptase (Life Technologies, AM2043) according to the manufacturer's instructions. The expression of autophagy genes was determined by RT-PCR using the Sybr Select Master Mix (Life Technologies, A25742) in a QuantStudio 6 Flex Real-Time PCR System (Life Technologies, France). Expression of mRNA was normalized to that of *Aip* and *Sf3a1* as house-keeping genes. Primers were purchased from Qiagen.

Western blot

Protein expression was evaluated on cell lysates obtained after exposure of macrophages to 50 µg/mL of particles for 6 h. Cell lysates were prepared by extracting proteins with RIPA lysis buffer (Sigma Aldrich, R0278) supplemented with protease inhibitors. Twenty-five µg of protein were separated via SDS-polyacrylamide gel electrophoresis and transferred to polyvinylidene difluoride (PVDF) membrane. The membrane was blocked with 5% non-fat dry milk in Tris-buffered saline (Sigma, T5912), and incubated with primary antibodies overnight at 4°C. The primary antibodies used in this study were: LAMP2 (Novus Biologicals, NB300-591), LC3 (MBL, PM036), LAMP1 (R&D Systems, MAB4320),

SNAPIN (ProteinTech, 10055-1-AP), ACTB/beta actin (Sigma Aldrich, A5441). ACTB was used as an internal standard. Quantification of the expression of each protein was obtained using the ratio to ACTB expression, and normalized to the ratio obtained in control conditions.

Confocal scanning immunofluorescence microscopy

Cells were exposed to 10 µg/ml of particles for 6 h and then fixed with freshly prepared 4 vol. % paraformaldehyde at 4°C for 20 min. The cells were then permeabilized with Triton X-100 (0.1 vol. % solution diluted in phosphate-buffered saline [PBS; Sigma, P5493]) during 10 min. For cytoskeleton structure analysis, cells were incubated with the anti-TUBA/α-tubulin primary antibody overnight at 4°C (Life Technologies, 236-10501) followed by an incubation of 1 h with an Alexa Fluor 488 rabbit anti-mouse IgG (green; Life Technologies, MA5-18127). For actin staining, cells were directly incubated with an Alexa Fluor 568 phalloidin (red; Life Technologies, A-11004) for 20 min. Colocalization of LC3 with LAMP1 was measured using anti-LC3 and anti-LAMP1 (R&D Systems, AF4320) antibodies. The slides were mounted with a coverslip using Prolong Gold mounting medium with DAPI (Life Technologies, P36974). Cell images were obtained using an LSM 510 META confocal microscope (Carl Zeiss).

mRFP-GFP-LC3 assay

To monitor autophagy flux, RAW 264.7 macrophages were transfected with mRFP-GFP-LC3 plasmid by nucleofection, using an Amaxa cell line nucleofector kit V for RAW 264.7 (Lonza, V4XC-2032) and following the manufacturer's instructions.

The following day, transfected cells were treated with 10 µg/ml of particles for 6 h. After treatment, the cells were fixed with 4 vol. % paraformaldehyde in PBS, and imaged

using an LSM 510 META confocal microscope (Carl Zeiss). Autophagy was measured by counting the cells presenting GFP-LC3 puncta or GFP^+ $mRFP^+$ (yellow, i.e. autophagosomes) and GFP^- $mRFP^-$ (red, i.e. autolysosomes) puncta. At least 30 cells/sample were counted for each condition, in at least 10 randomly selected fields.

LysoSensor assay

RAW 264.7 cells were exposed to 10 µg/mL CNT for 6 h. The cells were then stained with 2 µg/mL acridine orange (Sigma, A9231) for a period of 20 min at 37°C and 5% CO_2 [41]. After the incubation period, the cells were washed with PBS, followed by the addition of DMEM without serum to the cells. Immediately, the fluorescence images of the cells were digitally acquired on an LSM 510 META confocal microscope (Carl Zeiss).

Statistical analysis

Each value is given as the mean ± standard error of the mean (SEM) of at least 3 experiments. Data were analyzed with the commercially available software GraphPad (GraphPad Prism 5.01, GraphPad Software Inc, La Jolla, CA, USA). Comparisons between multiple groups were performed using Kruskall-Wallis' non-parametric analysis of variance test followed, when a difference was detected, by two-by-two comparisons with the Mann-Whitney's t test. P-values <0.05 were considered significant.

Competing interests

The authors declare no conflict of interest

Acknowledgements

This work was supported by the "Agence Nationale de la Recherche France" (Nanautophagie ANR-13-CESA-0010-01). The authors would like to acknowledge the support they obtained from DHU A-TVB (Département Hospital-Universitaire Ageing-Thorax Vessel Blood) and from the LabEx SERENADE (11-LABX-0064). VC is supported by a fellowship from C'Nano Ile-de-France. C'Nano-IdF is the nanoscience competence center of Paris Region, supported by the National Center for Scientific Resarch (CNRS), the Atomic Energy Commission (CEA), Ministère de l'Enseignement Supérieur et de la Recherche (MESR), and the Région Ile-de-France. MJL is supported by a fellowship from the French Agency for Food, Environmental and Occupational Health & Safety (ANSES). BA is supported by a post-doctoral grant from LabEx SERENADE. This work has benefited from the facilities and expertise of the Imagif Cell Biology Unit of the Gif campus which is supported by the Conseil Général de l'Essonne, as well as from the Imagery platform of IMRB (X. Decrouy).

References

1. Boczkowski J, Lanone S. Respiratory toxicities of nanomaterials - A focus on carbon nanotubes. Adv Drug Deliv Rev. 2012 May 26;64:1694-1699. doi: S0169-409X(12)00192-5 [pii]

10.1016/j.addr.2012.05.011. PubMed PMID: 22641117; Eng.

2. Shi H, Magaye R, Castranova V, et al. Titanium dioxide nanoparticles: a review of current toxicological data. Part Fibre Toxicol. 2013;10:15. doi: 1743-8977-10-15 [pii]

10.1186/1743-8977-10-15 [doi]. PubMed PMID: 23587290; eng.

3. Muller J, Huaux F, Moreau N, et al. Respiratory toxicity of multi-wall carbon nanotubes. Toxicol Appl Pharmacol. 2005 Sep 15;207(3):221-31. PubMed PMID: 16129115.
4. Park EJ, Yoon J, Choi K, et al. Induction of chronic inflammation in mice treated with titanium dioxide nanoparticles by intratracheal instillation. Toxicology. 2009 Jun 16;260(1-3):37-46. doi: S0300-483X(09)00136-X [pii]

10.1016/j.tox.2009.03.005. PubMed PMID: 19464567; eng.

5. Lanone S, Andujar P, Kermanizadeh A, et al. Determinants of carbon nanotube toxicity. Adv Drug Deliv Rev. 2013 Aug 6. doi: S0169-409X(13)00173-7 [pii]

10.1016/j.addr.2013.07.019. PubMed PMID: 23928473; Eng.

6. Shvedova AA, Kagan VE, Fadeel B. Close encounters of the small kind: adverse effects of man-made materials interfacing with the nano-cosmos of biological systems. Annu Rev Pharmacol Toxicol. 2010;50:63-88. doi: 10.1146/annurev.pharmtox.010909.105819. PubMed PMID: 20055698; eng.
7. Mizushima N, Yoshimori T, Levine B. Methods in mammalian autophagy research. Cell. 2010 Feb 5;140(3):313-26. doi: S0092-8674(10)00063-2 [pii]

10.1016/j.cell.2010.01.028. PubMed PMID: 20144757; eng.

8. Choi AMK, Ryter SW, Levine B. Autophagy in Human Health and Disease. New England Journal of Medicine. 2013;368(7):651-662. doi: doi:10.1056/NEJMra1205406. PubMed PMID: 23406030.
9. Nakahira K, Pabon Porras MA, Choi AMK. Autophagy in Pulmonary Diseases. American Journal of Respiratory and Critical Care Medicine. 2016. doi: 10.1164/rccm.201512-2468SO.
10. Cohignac V, Landry MJ, Boczkowski J, et al. Autophagy as a possible underlying mechanism of nanomaterial toxicity. Nanomaterials. 2014;4:548-582.
11. Stern ST, Adiseshaiah PP, Crist RM. Autophagy and lysosomal dysfunction as emerging mechanisms of nanomaterial toxicity. Part Fibre Toxicol. 2012 Jun 14;9(1):20. doi: 1743-8977-9-20 [pii]

10.1186/1743-8977-9-20. PubMed PMID: 22697169; Eng.

12. Yu KN, Kim JE, Seo HW, et al. Differential toxic responses between pristine and functionalized multiwall nanotubes involve induction of autophagy accumulation in murine lung. J Toxicol Environ Health A. 2013;76(23):1282-92. doi: 10.1080/15287394.2013.850137. PubMed PMID: 24283420; eng.
13. Ma X, Wu Y, Jin S, et al. Gold nanoparticles induce autophagosome accumulation through size-dependent nanoparticle uptake and lysosome impairment. ACS Nano. 2011 Nov 22;5(11):8629-39. doi: 10.1021/nn202155y. PubMed PMID: 21974862; eng.

14. Mittal S, Sharma PK, Tiwari R, et al. Impaired lysosomal activity mediated autophagic flux disruption by graphite carbon nanofibers induce apoptosis in human lung epithelial cells through oxidative stress and energetic impairment [journal article]. Particle and Fibre Toxicology. 2017 April 28;14(1):15. doi: 10.1186/s12989-017-0194-4.
15. Orecna M, Paoli SH, Janouskova O, et al. Toxicity of carboxylated carbon nanotubes in endothelial cells is attenuated by stimulation of the autophagic flux with the release of nanomaterial in autophagic vesicles. Nanomed Nanotech Biol Med. 2014;10. doi: 10.1016/j.nano.2014.02.001.
16. Bussy C, Paineau E, Cambedouzou J, et al. Intracellular fate of carbon nanotubes inside murine macrophages: pH-dependent detachment of iron catalyst nanoparticles. Part Fibre Toxicol. 2013 Jun 25;10(1):24. doi: 1743-8977-10-24 [pii]

10.1186/1743-8977-10-24 [doi]. PubMed PMID: 23800198; Eng.
17. Yu JX, Li TH. Distinct biological effects of different nanoparticles commonly used in cosmetics and medicine coatings. Cell Biosci. 2011;1(1):19. doi: 2045-3701-1-19 [pii]

10.1186/2045-3701-1-19. PubMed PMID: 21711940; eng.
18. Landry M, Pinault M, Tchankouo S, et al. Early signs of multi-walled carbon nanotbues degradation in macrophages, via an intracellular pH-dependent biological mechanism; importance of length and functionalization. Part Fibre Toxicol. 2016 Nov 24;13(1):61. doi: 10.1186/s12989-016-0175-z. PubMed PMID: 27881140; PubMed Central PMCID: PMCPMC5122009.
19. Kimura S, Noda T, Yoshimori T. Dissection of the autophagosome maturation process by a novel reporter protein, tandem fluorescent-tagged LC3. Autophagy. 2007;3:452-460.
20. Mackeh R, Perdiz D, Lorin S, et al. Autophagy and microtubules - new story, old players. J Cell Sci. 2013 Mar 1;126(Pt 5):1071-80. doi: 126/5/1071 [pii]

10.1242/jcs.115626 [doi]. PubMed PMID: 23620510; eng.
21. Shen H-M, Mizushima N. At the end of the autophagic road: an emerging understanding of lysosomal functions in autophagy. Trends in Biochemical Sciences.39(2):61-71. doi: 10.1016/j.tibs.2013.12.001.
22. Ganley IG. Autophagosome maturation and lysosomal fusion. Essays in biochemistry. 2013;55:65-78. doi: 10.1042/bse0550065. PubMed PMID: 24070472.
23. Shi B, Huang Q-Q, Birkett R, et al. SNAPIN is critical for lysosomal acidification and autophagosome maturation in macrophages. Autophagy. 2017 2017/02/01;13(2):285-301. doi: 10.1080/15548627.2016.1261238.
24. Ishidoh K, Takeda-Ezaki M, Watanabe S, et al. Analysis of where and which types of proteinases participate in lysosomal proteinase processing using bafilomycin A1 and Helicobacter pylori Vac A toxin. Journal of biochemistry. 1999 Apr;125(4):770-9. PubMed PMID: 10101291; eng.
25. Mu Q, Jiang G, Chen L, et al. Chemical basis of interactions between engineered nanoparticles and biological systems. Chem Rev. 2014 Aug 13;114(15):7740-81. doi: 10.1021/cr400295a. PubMed PMID: 24927254; PubMed Central PMCID: PMCPMC4578874. eng.
26. Wan B, Wang ZX, Lv QY, et al. Single-walled carbon nanotubes and graphene oxides induce autophagosome accumulation and lysosome impairment in primarily cultured murine peritoneal macrophages. Toxicol Lett. 2013 Jun 13;221(2):118-127. doi: 10.1016/j.toxlet.2013.06.208. PubMed PMID: 23769962; Eng.

27. Klionsky DJ, Abdalla FC, Abeliovich H, et al. Guidelines for the use and interpretation of assays for monitoring autophagy. Autophagy. 2012;8. doi: 10.4161/auto.19496.
28. Kanno S, Hirano S, Chiba S, et al. The role of Rho-kinases in IL-1beta release through phagocytosis of fibrous particles in human monocytes. Arch Toxicol. 2015 Jan;89(1):73-85. doi: 10.1007/s00204-014-1238-2. PubMed PMID: 24760326; eng.
29. Dong Y, Sun H, Li X, et al. Impact of Carbon Nanomaterials on Actin Polymerization. J Nanosci Nanotechnol. 2016 Mar;16(3):2408-17. PubMed PMID: 27455649; eng.
30. Ilardi JM, Mochida S, Sheng ZH. Snapin: a SNARE-associated protein implicated in synaptic transmission. Nature neuroscience. 1999 Feb;2(2):119-24. doi: 10.1038/5673. PubMed PMID: 10195194; eng.
31. Shi B, Huang Q, Tak PP, et al. SNAPIN: an endogenous toll-like receptor ligand in rheumatoid arthritis. Annals of the rheumatic diseases. 2012;71(8):1411-1417. doi: 10.1136/annrheumdis-2011-200899.
32. Farrera C, Fadeel B. It takes two to tango: Understanding the interactions between engineered nanomaterials and the immune system. European Journal of Pharmaceutics and Biopharmaceutics. 2015 2015/09/01/;95:3-12. doi: http://dx.doi.org/10.1016/j.ejpb.2015.03.007.
33. Cui Y, Liu H, Zhou M, et al. Signaling pathway of inflammatory responses in the mouse liver caused by TiO2 nanoparticles. J Biomed Mater Res A. 2011 Jan;96(1):221-9. doi: 10.1002/jbm.a.32976. PubMed PMID: 21105171; eng.
34. Ze Y, Sheng L, Zhao X, et al. TiO2 nanoparticles induced hippocampal neuroinflammation in mice. PLoS One. 2014;9(3):e92230. doi: 10.1371/journal.pone.0092230. PubMed PMID: 24658543; PubMed Central PMCID: PMCPMC3962383. eng.
35. Hiraku Y, Guo F, Ma N, et al. Multi-walled carbon nanotube induces nitrative DNA damage in human lung epithelial cells via HMGB1-RAGE interaction and Toll-like receptor 9 activation [journal article]. Particle and Fibre Toxicology. 2016 March 29;13(1):16. doi: 10.1186/s12989-016-0127-7.
36. Castro C, Pinault M, Porterat D, et al. The role of hydrogen in the aerosol-assisted chemical vapor deposition process in producing thin and densely packed vertically aligned carbon nanotubes. Carbon. 2013 9//;61:585-594. doi: http://dx.doi.org/10.1016/j.carbon.2013.05.040.
37. Glory J, Mierczynska A, Pinault M, et al. Dispersion study of long and aligned multi-walled carbon nanotubes in water. J Nanosci Nanotechnol. 2007 Oct;7(10):3458-62. PubMed PMID: 18330157; eng.
38. Ishida T, Kinoshita N, Okatsu H, et al. Influence of the Support and the Size of Gold Clusters on Catalytic Activity for Glucose Oxidation. Angewandte Chemie International Edition. 2008;47(48):9265-9268. doi: 10.1002/anie.200802845.
39. Armand L, Dagouassat M, Belade E, et al. Titanium dioxide nanoparticles induce matrix metalloprotease 1 in human pulmonary fibroblasts partly via an interleukin-1β-dependent mechanism. Am J Respir Cell Mol Biol. 2013;48. doi: 10.1165/rcmb.2012-0099OC.
40. Posadas I, De Rosa S, Carmen Terencio M, et al. Cacospongionolide B suppresses the expression of inflammatory enzymes and tumour necrosis factor-α by inhibiting nuclear factor-κB activation. British Journal of Pharmacology. 2003;138(8):1571-1579. doi: 10.1038/sj.bjp.0705189.
41. Yue W, Hamai A, Tonelli G, et al. Inhibition of the autophagic flux by salinomycin in breast cancer stem-like/progenitor cells interferes with their maintenance. Autophagy.

2013 May;9(5):714-29. doi: 10.4161/auto.23997. PubMed PMID: 23519090; PubMed Central PMCID: PMCPMC3669181. eng.

Table 1. Physico-chemical characteristics of the particles used

	Full description	**Size**	**Crystal phase**	**Surface area** (m^2/g)	**Zeta potential in water pH 7** (mV)	**Hydrodynamic diameter in water** (nm)	**Intrinsic ROS production**
S-CNT	Short CNT	*26 nm x1.7 µm*	*N/A*	62	8	/	++
SF-CNT	Short functionalized CNT	*25 nm x1.6 µm*	*N/A*	62	8	/	*ND*
L-CNT	Long CNT	*24 nm x6.4 µm*	*N/A*	62	8	/	++
LF-CNT	Long functionalized CNT	*25 nm x9.2 µm*	*N/A*	62	8	/	++
FW2	Carbon black	*13 nm*	*Amorphous*	*373*	*-11.9*	*1033 ± 88*	ND
Micro	Micrometric TiO_2	*200 nm*	*Anatase*	*8*	*0.4*	*874 ± 149*	+
A10	Nanometric TiO_2 (Anatase)	*10 nm*	*Anatase*	*96*	*-2.1*	*1020 ±146*	+
A/R	Nanometric TIO_2 (Anatase:Rutile mix)	*25-75 nm*	*Anatase:rutile (13:7)*	*27*	*0.2*	*715 ± 104*	+
Rut	Nanometric TiO_2 (Rutile)	5x20 nm	Rutile	160	-39.8	55 ± 20	ND
P25	Nanometric TiO_2 (Pristine)	30 nm	Anatase rutile (4:1)	50	-7.3	48 ± 19	+
P25 - Au3	Nanometric TiO_2 (grafted with 3-nm-Au NP)	30 nm	Anatase rutile (4:1)	57	-21.1	175 ± 103	+
P25 - Au8	Nanometric TiO_2 (grafted with 8-nm-Au NP)	30 nm	Anatase rutile (4:1)	57	-21.9	54 ± 34	+

Data are given as mean±standard deviation when applicable. ND, not detectable; /, not done; +, low ROS production; ++, high ROS production. Data in italics have already been published [18, 39].

Legend to figures

Figure 1. Transmission electron microscopy (TEM) images of particles and macrophages exposed to particles. (**A**) TEM images of the particles. Scale bar: 50 nm. (**B**) TEM images of RAW 264.7 macrophages exposed to 50 µg/mL of particles for 6 h. Scale bar: 500 nm. Black arrows point towards particles.

Figure 2. Quantification of autophagy markers and autophagy flux. (**A**) Representative western blot images of LC3 in RAW 264.7 macrophages exposed to 50 µg/mL particles for 6 h. ACTB was used as loading control. (**B**) Quantification of LC3-II protein expression levels. (**C**) Representative western blot images of LC3 in RAW 264.7 macrophages exposed to 50 µg/mL of particles for 6 h in the presence or absence of Baf-A1 (final concentration: 100 nM). ACTB was used as a loading control. (**D**) Quantification of protein expression levels for LC3-II. Data are given as mean ± SEM. *, $p<0.05$ *versus* control condition.

Figure 3. Quantification of autophagy flux. (**A**) Confocal images of the transfected mRFP-GFP-LC3 plasmid in RAW 264.7 macrophages exposed to 10 µg/mL of particles for 6 h. Scale bar: 10 µm. Yellow puncta: autophagosomes; red puncta: autolysosomes. (**B**) Quantification of autophagosome and autolysosome number per cell in each condition. More than 30 cells were counted in each condition. Data are given as mean ± SEM. *, $p<0.05$ *versus* control condition. Baf, Baf-A1 (100 nM); Rapa, rapamycin (100 nM).

Figure 4. Quantification of LC3-LAMP1 colocalization. (**A**) Confocal images of RAW264.7 macrophages exposed to 10 µg/ml particles for 6 h. Cells were stained with antibodies against

LC3 (green) and LAMP1 (red). Scale bar: 5 µm. Arrowheads indicate colocalization of LC3 and LAMP1 staining, attesting to the fusion between autophagosomes (LC3) and lysosomes (LAMP1). (**B**) Quantification of LC3-LAMP1 colocalization. Data are given as mean ± SEM. *, $p<0.05$ *versus* control condition.

Figure 5. Analysis of lysosomal alterations. (**A**) Fluorescence images of RAW264.7 macrophages exposed to 10 µg/ml particles for 6 h. Cells were incubated with acridine orange dye. Scale bar: 5 µm. Data are given as mean ± SEM. *, $p<0.05$ *versus* control condition.

Figure 6. Quantification of SNAPIN expression. (**A**) Representative western blot images of SNAPIN in RAW 264.7 macrophages exposed to 50 µg/mL of particles for 6 h. ACTB was used as a loading control. (**B**) Quantification of protein expression levels for SNAPIN. Data are given as mean ± SEM. *: $p<0.05$ *versus* control condition.

Supplementary information

Table S1. Zeta potential in culture medium.

	Zeta potential in culture medium (mV)
FW2	-10.0
Micro	-8.3
A10	6.1
A/R	1.6
Rut	-16.1
P25	12.4
P25 - Au3	18.4
P25 - Au8	19.9

Figure S1. Phagocytic activity of macrophages exposed to particles. Quantification of RAW 264.7 phagocytic activity exposed to 50 µg/ml particles for 6 h. Data are given as mean ± SEM. *, $p<0.05$ *versus* control condition; **, $p<0.01$ *versus* control condition.

Figure S2. Viability of macrophages exposed to particles. Quantification of cell viability in RAW 264.7 macrophages exposed to 10-100 µg/mL particles for 6 h, by WST-1 (**A**) or Hoechst assay (**B**). Results are expressed as percentage of values obtained for the control condition (untreated cells). Data are given as mean ± SEM. *: $p<0.05$ *versus* control condition.

Figure S3. Quantification of LC3 expression in primary macrophages. (**A**) Representative western blot images of LC3 in primary macrophages exposed to 50 µg/mL of particles for 6 h in the presence or absence of bafilomycin A_1 (Baf A1, final concentration: 100 nM). Actin was used as a loading control. (**B**) Quantification of protein expression levels for LC3-II. Data are given as mean ± SEM. *, $p<0.05$ *versus* control condition.

Figure S4. Quantification of SQSTM1/p62 expression in RAW macrophages. (**A**) Representative western blot images of SQSTM1 in RAW 264.7 macrophages exposed to 50 µg/mL particles for 6 h. Actin was used as a loading control. (**B**) Quantification of SQSTM1 protein expression levels. Data are given as mean ± SEM. *, $p<0.05$ *versus* control condition.

Figure S5. Cytoskeleton analysis. Confocal images of RAW264.7 macrophages exposed to 10 µg/ml particles for 6 h. Cells were stained with the anti-TUBA/α-tubulin (Panel **A**) or actin (Panel **B**) antibody. Scale bar: 5 µm. Noco, nocodazole (positive control, 15 µg/ml).

Figure S6. Evaluation of lysosomal number. (**A**) Representative western blot images of LAMP1 and LAMP2 in RAW 264.7 macrophages exposed to 50 µg/mL particles for 6 h. Actin was used as a loading control. (**B-C**) Quantification of protein expression levels for LAMP1 (**B**), or LAMP2 (**C**). Data are given as mean ± SEM. *, $p<0.05$ *versus* control condition; **, $p<0.01$ *versus* control condition.

Figure 1

A

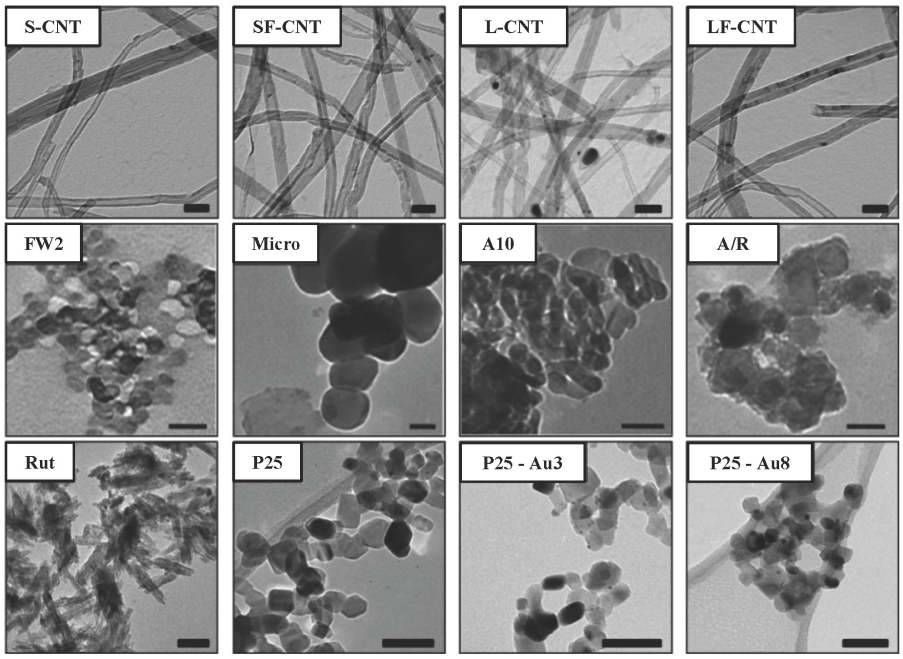
S-CNT
SF-CNT
L-CNT
LF-CNT
FW2
Micro
A10
A/R
Rut
P25
P25 - Au3
P25 - Au8

B

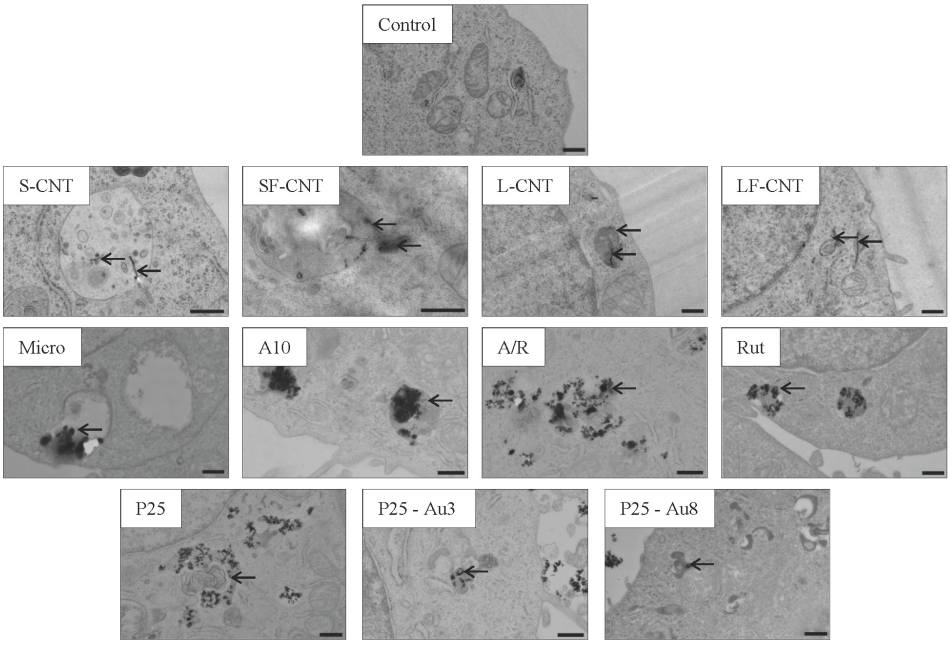
Control
S-CNT
SF-CNT
L-CNT
LF-CNT
Micro
A10
A/R
Rut
P25
P25 - Au3
P25 - Au8

Figure 2

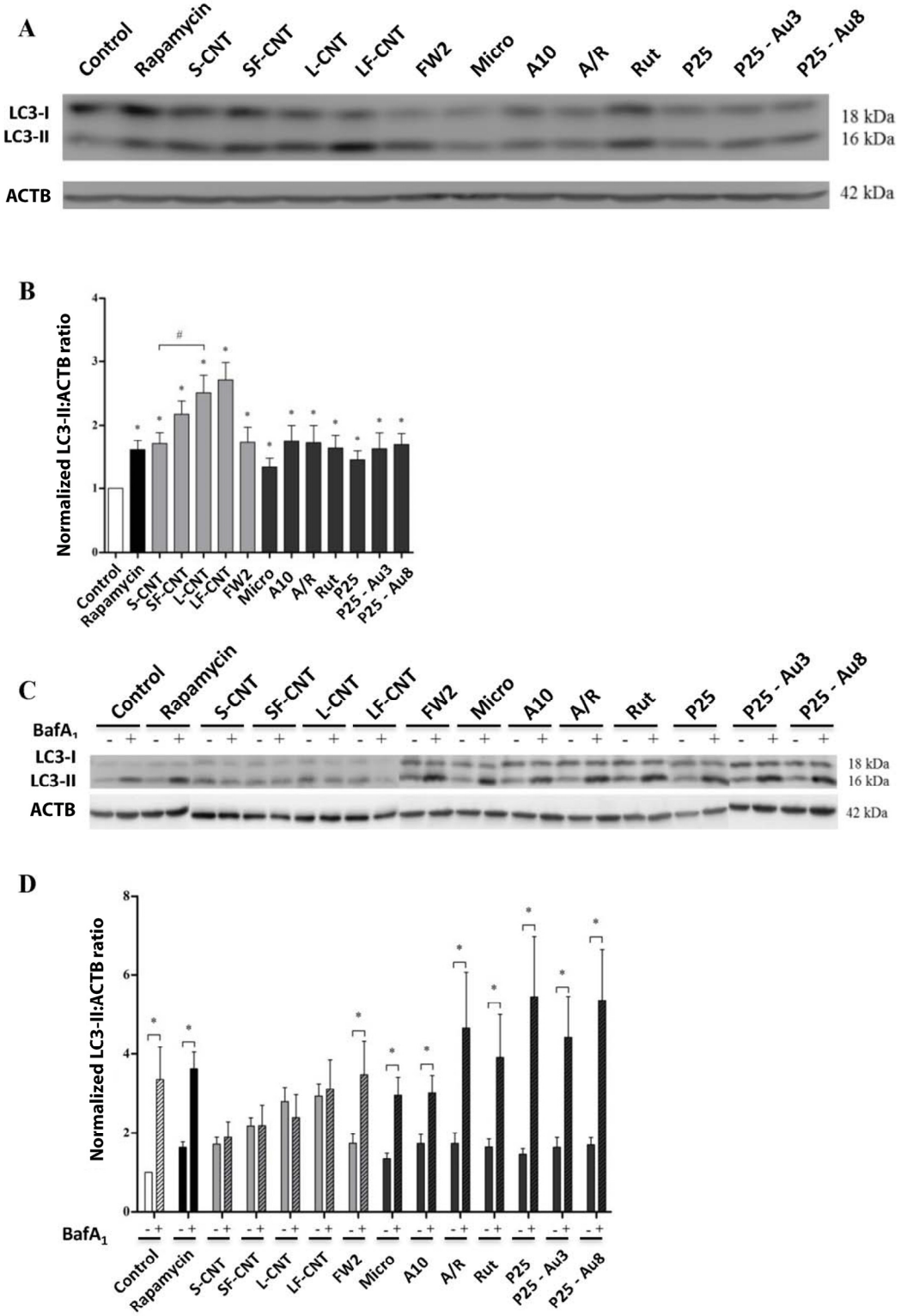
A
Control
Rapamycin
S-CNT
SF-CNT
L-CNT
LF-CNT
FW2
Micro
A10
A/R
Rut
P25
P25 - Au3
P25 - Au8
LC3-I
LC3-II
18 kDa
16 kDa
ACTB
42 kDa
B
Normalized LC3-II:ACTB ratio
C
BafA1
D
Normalized LC3-II:ACTB ratio

Figure 3

A

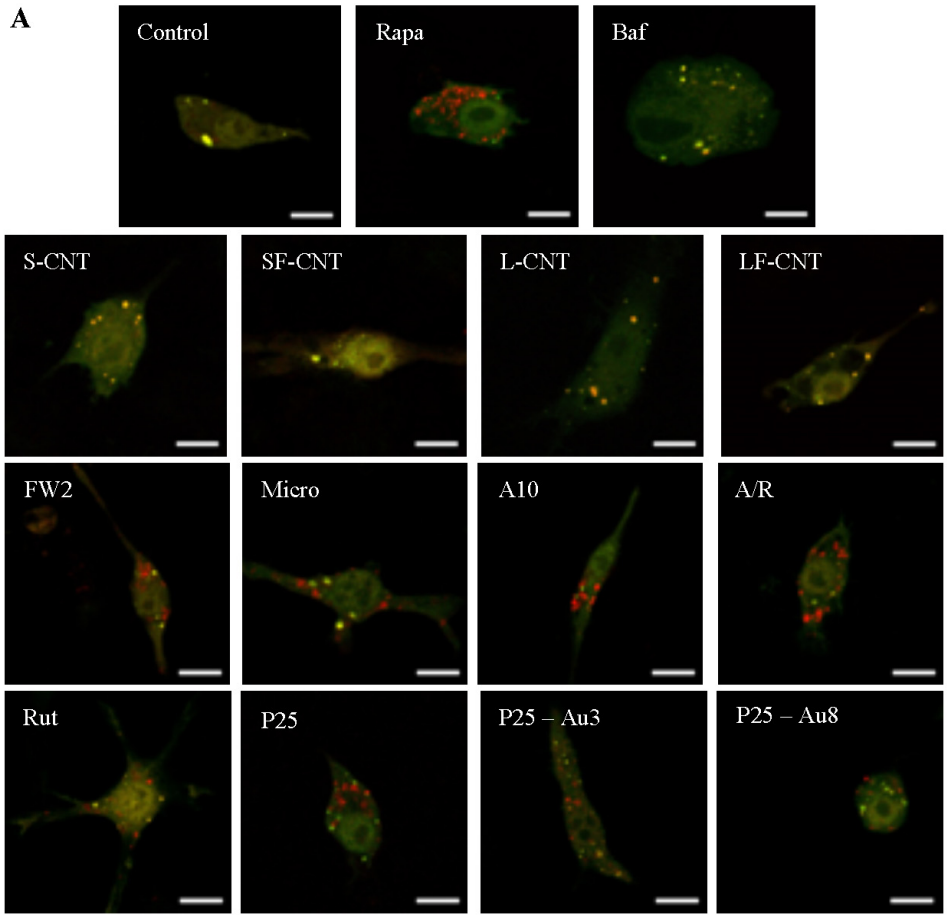
Control
Rapa
Baf
S-CNT
SF-CNT
L-CNT
LF-CNT
FW2
Micro
A10
A/R
Rut
P25
P25 – Au3
P25 – Au8

B

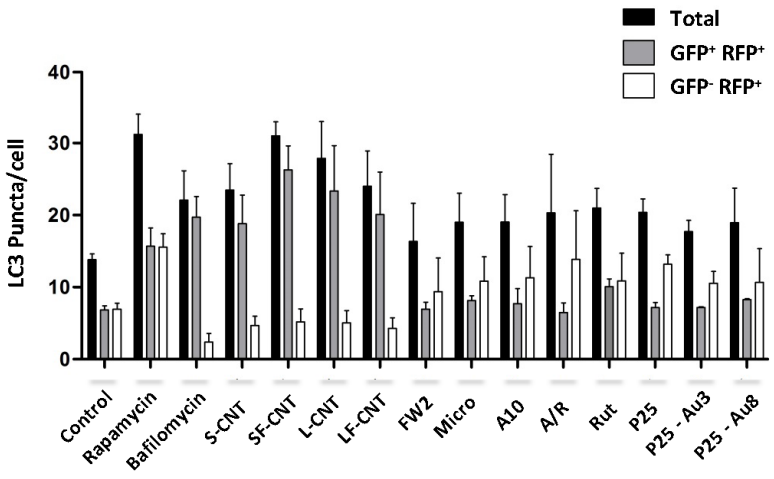
Total
GFP+ RFP+
GFP- RFP+
LC3 Puncta/cell
40
30
20
10
0
Control
Rapamycin
Bafilomycin
S-CNT
SF-CNT
L-CNT
LF-CNT
FW2
Micro
A10
A/R
Rut
P25
P25 - Au3
P25 - Au8

Figure 4

A

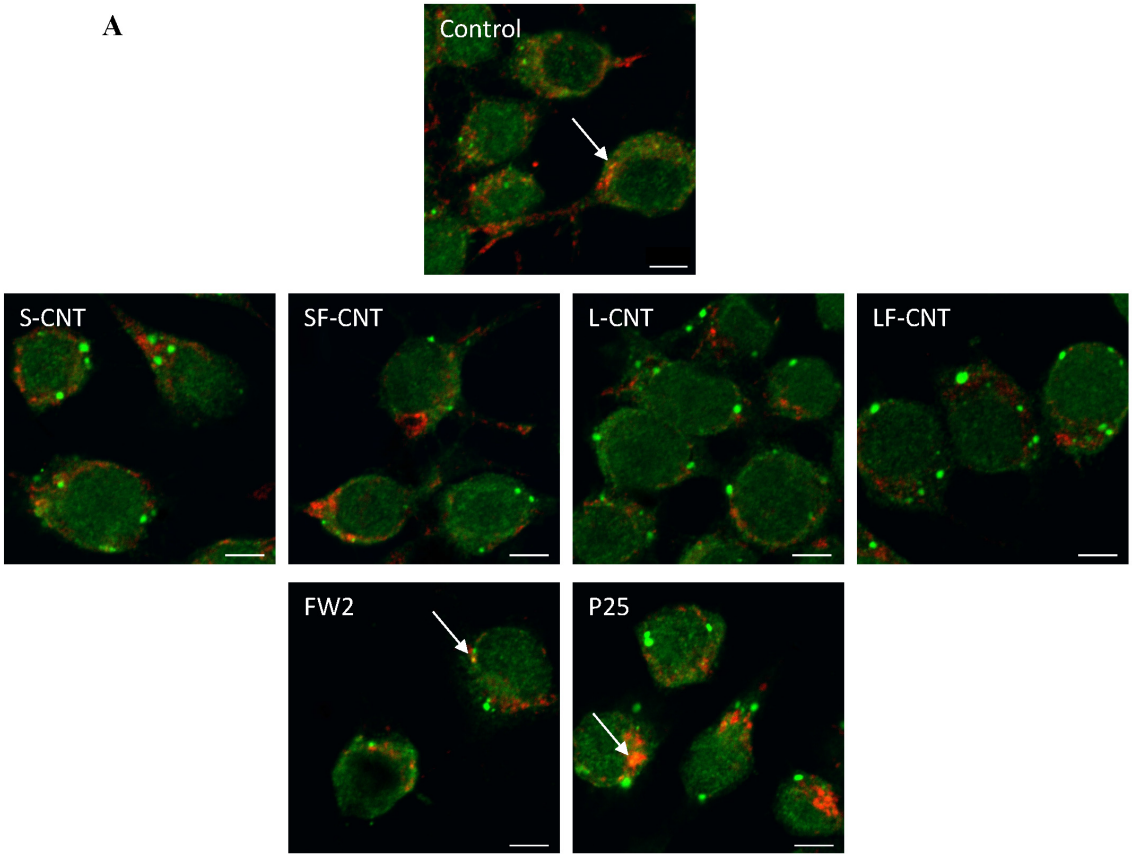
Control
S-CNT
SF-CNT
L-CNT
LF-CNT
FW2
P25

B

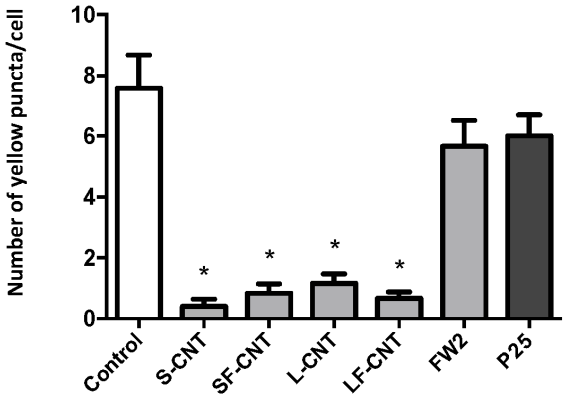
Number of yellow puncta/cell
10
8
6
4
2
0
*
*
*
*
Control
S-CNT
SF-CNT
L-CNT
LF-CNT
FW2
P25

Figure 5

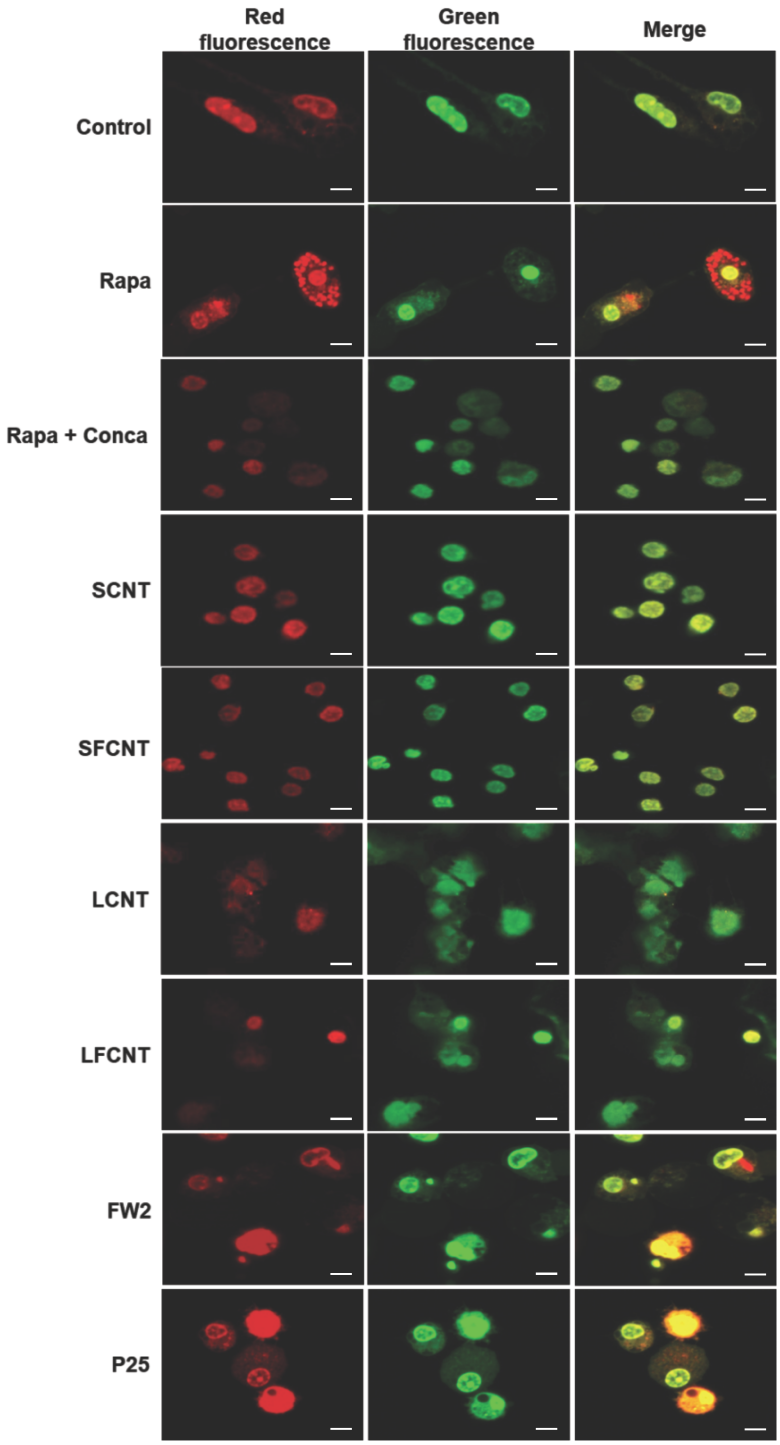
Red fluorescence
Green fluorescence
Merge
Control
Rapa
Rapa + Conca
SCNT
SFCNT
LCNT
LFCNT
FW2
P25

Figure 6

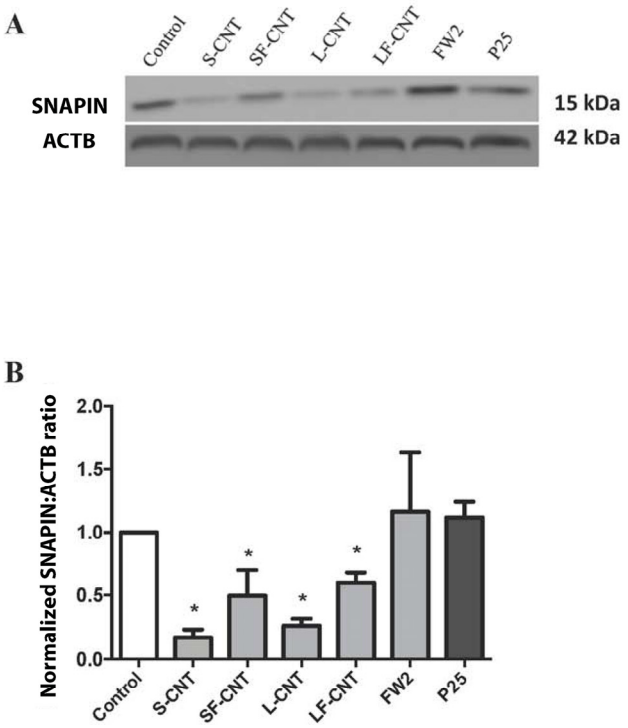
A
Control
S-CNT
SF-CNT
L-CNT
LF-CNT
FW2
P25
SNAPIN
ACTB
15 kDa
42 kDa
B
Normalized SNAPIN:ACTB ratio
2.0
1.5
1.0
0.5
0.0
*
*
*
*
Control
S-CNT
SF-CNT
L-CNT
LF-CNT
FW2
P25

Figure S1

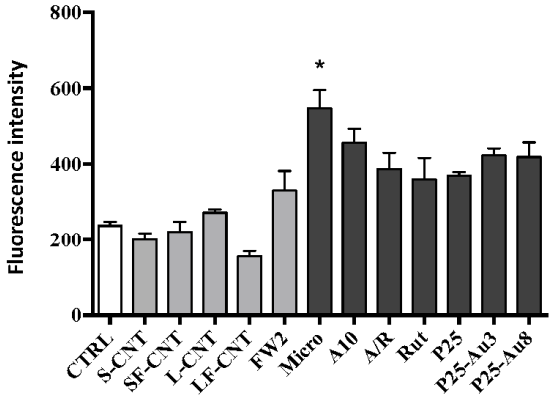
Fluorescence intensity
800
600
400
200
0
*
CTRL
S-CNT
SF-CNT
L-CNT
LF-CNT
FW2
Micro
A10
A/R
Rut
P25
P25-Au3
P25-Au8

Figure S2

A

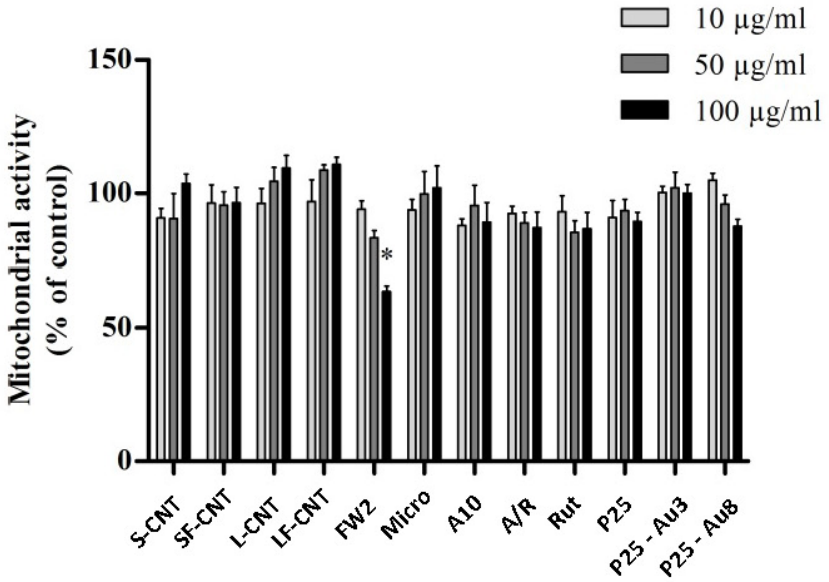
10 µg/ml
50 µg/ml
100 µg/ml
Mitochondrial activity
(% of control)
150
100
50
0
*
S-CNT
SF-CNT
L-CNT
LF-CNT
FW2
Micro
A10
A/R
Rut
P25
P25 - Au3
P25 - Au8

B

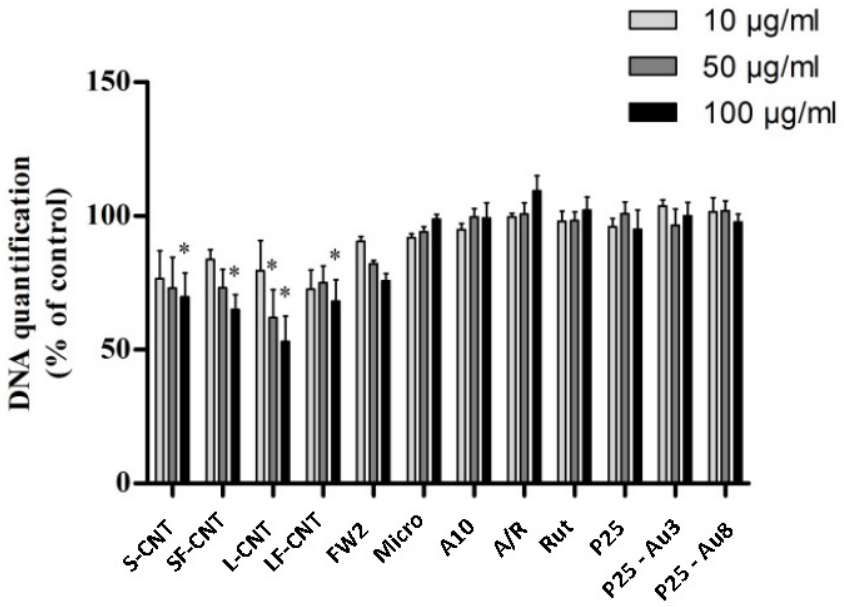
10 µg/ml
50 µg/ml
100 µg/ml
DNA quantification
(% of control)
150
100
50
0
*
S-CNT
SF-CNT
L-CNT
LF-CNT
FW2
Micro
A10
A/R
Rut
P25
P25 - Au3
P25 - Au8

Figure S3

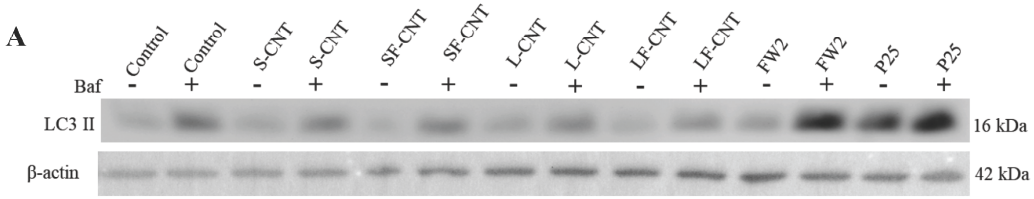
A
Control
Control
S-CNT
S-CNT
SF-CNT
SF-CNT
L-CNT
L-CNT
LF-CNT
LF-CNT
FW2
FW2
P25
P25
Baf
- + - + - + - + - + - + - +
LC3 II
16 kDa
β-actin
42 kDa

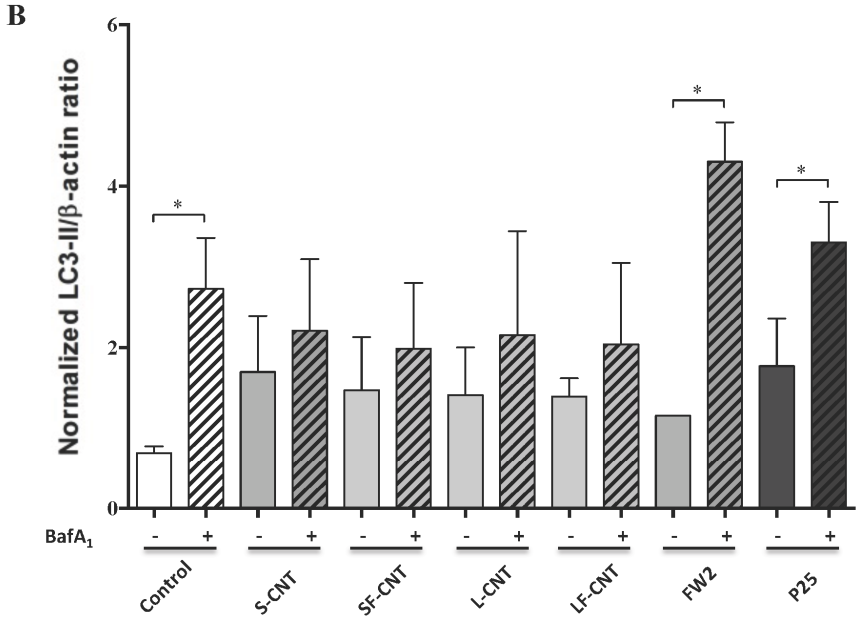
B
Normalized LC3-II/β-actin ratio
6
4
2
0
*
*
*
BafA1
- + - + - + - + - + - + - +
Control
S-CNT
SF-CNT
L-CNT
LF-CNT
FW2
P25

Figure S4

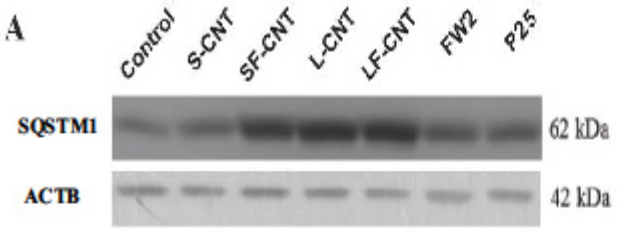
A
Control
S-CNT
SF-CNT
L-CNT
LF-CNT
FW2
P25
SQSTM1
62 kDa
ACTB
42 kDa

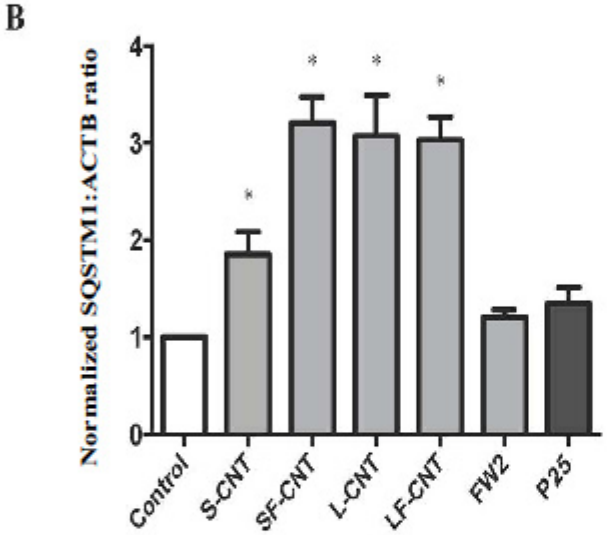
B
Normalized SQSTM1:ACTB ratio
0
1
2
3
4
*
*
*
*
Control
S-CNT
SF-CNT
L-CNT
LF-CNT
FW2
P25

Figure S5

A

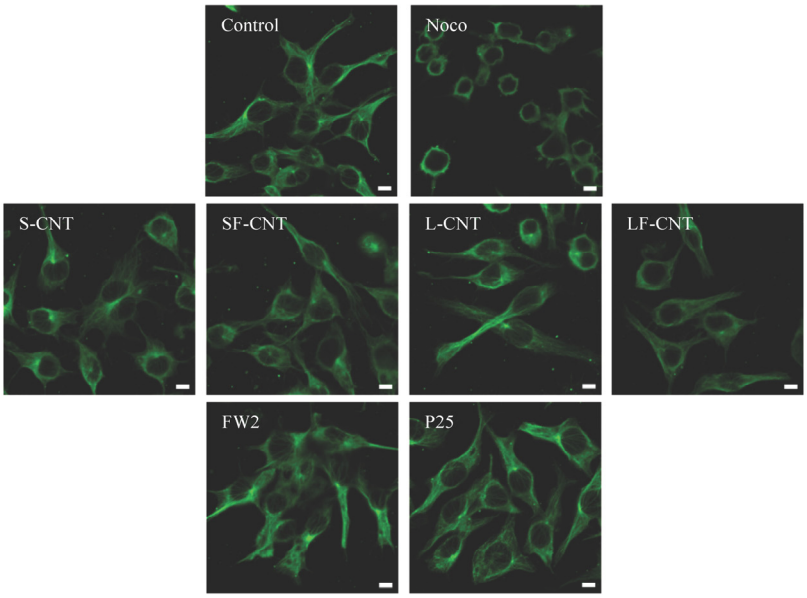
Control
Noco
S-CNT
SF-CNT
L-CNT
LF-CNT
FW2
P25

B

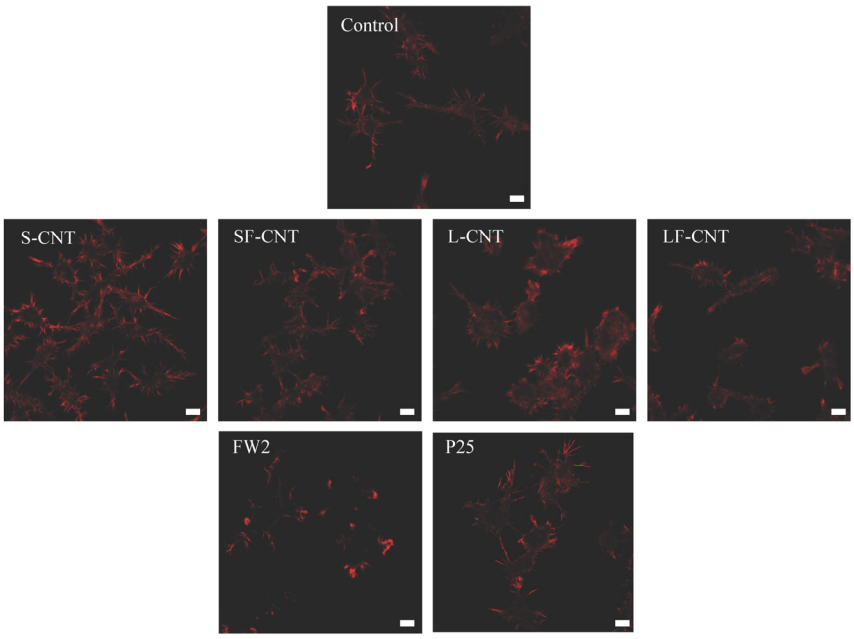
Control
S-CNT
SF-CNT
L-CNT
LF-CNT
FW2
P25

Figure S6

A

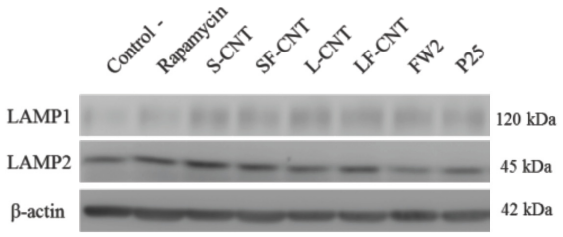

B

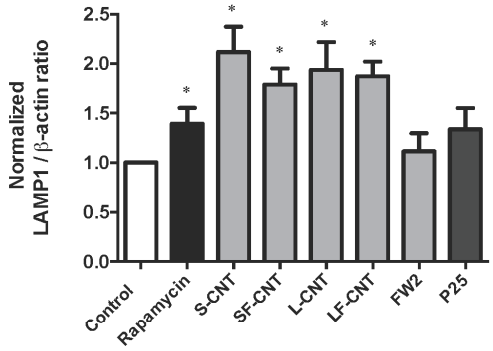
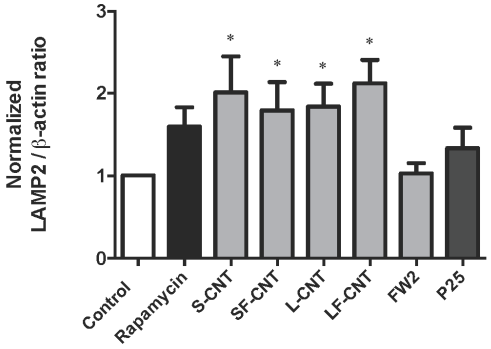
C